Biogeosciences Discuss., 10, 11343–11373, 2013
www.biogeosciences-discuss.net/10/11343/2013/
doi:10.5194/bgd-10-11343-2013

Biogeosciences Discussions
Open Access

Sensitivity of pelagic $CaCO_3$ dissolution to ocean acidification in an ocean biogeochemical model

A. Regenberg[1], **B. Schneider**[1], **and R. Gangstø**[2,*]

[1]Institute of Geosciences, Christian-Albrechts University, Kiel, Germany
[2]Climate and Environmental Physics, Physics Institute, University of Bern, Bern, Switzerland
[*]now at: The Norwegian Meteorological Institute, Oslo, Norway

Received: 3 June 2013 – Accepted: 20 June 2013 – Published: 9 July 2013

Correspondence to: A. Regenberg (ar@gpi.uni-kiel.de)

Published by Copernicus Publications on behalf of the European Geosciences Union.

Abstract

In ocean biogeochemical models pelagic $CaCO_3$ dissolution is usually calculated as $R = k * S^n$, where k is the dissolution rate constant transforming S, the degree of (under-) saturation of seawater with respect to $CaCO_3$, into a time dependent rate R, and n is the reaction rate order. Generally, there are two ways to define the saturation state of seawater with respect to $CaCO_3$: (1) $\Delta[CO_3^{2-}]$, which reflects the difference between the in-situ carbonate ion concentration and the saturation concentration, and (2) Ω, which is approximated by the ratio of in-situ carbonate ion concentration over the saturation concentration. Although describing the same phenomenon, the deviation from equilibrium, both expressions are not equally applicable for the calculation of $CaCO_3$ dissolution in the ocean across pressure gradients, as they differ in their sensitivity to ocean acidification (change of $[CO_3^{2-}]$) over depth. In the present study we use a marine biogeochemical model to test the sensitivity of pelagic $CaCO_3$ dissolution to ocean acidification (1–4 × CO_2 + stabilization), exploring the possible parameter space for $CaCO_3$ dissolution kinetics as given in the literature. We find that at the millennial time scale there is a wide range of $CaCO_3$ particle flux attenuation into the ocean interior (e.g. a reduction of −55 to −85 % at 1000 m depth), which means that there are significant differences in the impact on particle ballasting, depending on the kinetic expression applied.

1 Introduction

1.1 Ocean acidification

The global ocean has currently taken up about 25 % of anthropogenic CO_2 emissions (Canadell et al., 2007). Due to the reaction of CO_2 with sea water the carbonate ion concentration ($[CO_3^{2-}]$) is reduced, which is followed by a decrease in pH. This process, termed ocean acidification, has already lowered the surface ocean pH by 0.1

BGD
10, 11343–11373, 2013

units compared to preindustrial values and it is predicted to proceed, affecting also the deep ocean as CO_2 emissions continue (Caldeira and Wickett, 2003). Ocean acidification was shown to be harmful for marine life such as calcifying phytoplankton and zooplankton organisms as well as corals (Schiebel, 2002; Kleypas et al., 2006; Fabry et al., 2008), bearing the risk of undesirable effects on the marine food chain and ocean carbon cycling with potential repercussions on atmospheric CO_2 and thus on climate (Barker et al., 2003; Hofmann and Schnellnhuber, 2009). While sensitivities and thresholds for the calcification of marine organisms are presently under debate (Riebesell, 2000; Langer et al., 2006; Iglesias-Rodriguez et al., 2008; Gangstø et al., 2011; Bach et al., 2012; Lohbeck et al., 2012), the effects on the chemical equilibrium of sea water, especially in the deep ocean which governs the attenuation time scale of the anthropogenic CO_2 perturbation by dissolution of $CaCO_3$ from sediments, can be estimated relatively easily by thermodynamic considerations of the well described marine carbonate system (Zeebe and Wolf-Gladrow, 2001). The saturation state of sea water with respect to $CaCO_3$ is the ultimate physico-chemical control determining whether $CaCO_3$ preservation or dissolution will take place.

About half of the anthropogenic carbon emissions will be taken up by the ocean in the future, due to the solubility of CO_2 in sea water (Sundquist, 1990) with an equilibration time scale on the order of 300 yr (Archer, 2005). On the long-term perspective (10^4–10^6 yr), the anthropogenic CO_2 perturbation will mostly be compensated by dissolution of $CaCO_3$ from marine sediments (Archer, 2005). Although anthropogenic CO_2 invades the ocean through the sea surface, deep ocean biota and marine sediments are particularly concerned, since abyssal $CaCO_3$ saturation levels are already low (Key et al., 2004). These naturally more acidic conditions are caused by the high amount of respiratory CO_2 and the increasing solubility of $CaCO_3$ with pressure (depth), so that even a minor change in the ocean's interior [CO_3^{2-}] may have profound effects, for example causing a switch from over- to undersaturated conditions. The resulting rise of the $CaCO_3$ saturation horizon would then be triggering sediment dissolution.

BGD
10, 11343–11373, 2013

Consequently, from the perspective of marine $CaCO_3$ sediments, ocean acidification is a process that more or less slowly proceeds from below (Gehlen et al., 2007).

Today, anthropogenic CO_2 in the ocean can be detected down to 3000 m water depth in the North Atlantic, following the path of North Atlantic Deep Water. In the South Pacific and Southern Indian Ocean it penetrates down to 1500 m via subduction of intermediate waters (Sabine et al., 2004). In all these ocean basins, which contain $CaCO_3$ rich sediments (Archer, 1996), anthropogenic CO_2 is thus approaching the depth of the $CaCO_3$ saturation horizons (Feely et al., 2004). Consequently, carbonate compensation will most probably take place here and it is likely to start soon (Gehlen et al., 2008).

1.2 Sensitivity of the sea water $CaCO_3$ saturation state to ocean acidification

To assess the impact of ocean acidification on the dissolution of marine carbonates and the resulting attenuation time scale of the anthropogenic CO_2 perturbation, an unambiguous measure is required that quantifies ongoing as well as expected changes in the marine carbonate system. Generally, there are two ways to approximate the saturation state of sea water with respect to $CaCO_3$:

$$\Delta[CO_3^{2-}] = [CO_3^{2-}] - [CO_3^{2-}]_{sat} \quad (1)$$

$$\Omega = [CO_3^{2-}]/[CO_3^{2-}]_{sat}, \quad (2)$$

where $[CO_3^{2-}]_{sat}$ refers to the solubility of $CaCO_3$. It is a function of temperature, salinity, and pressure, increasing over depth in the water column (thick black line in Fig. 1a). Supersaturation prevails when $\Delta[CO_3^{2-}]$ is positive and Ω above one, respectively, allowing $CaCO_3$ to precipitate. On the other hand, a negative $\Delta[CO_3^{2-}]$, which corresponds to Ω between zero and one, indicates that the respective water mass is undersaturated, driving $CaCO_3$ dissolution. Since both expressions ($\Delta[CO_3^{2-}]$, Ω) refer to the same phenomenon, i.e. the deviation of the in-situ $[CO_3^{2-}]$ from saturation, they are regarded as equivalent and usually Ω is applied to describe the degree of $CaCO_3$ saturation of

BGD
10, 11343–11373, 2013

a water parcel (Zeebe and Wolf-Gladrow, 2001). However, in contrast to $\Delta[CO_3^{2-}]$, the sensitivity of Ω to ocean acidification, i.e. a change in $[CO_3^{2-}]$, decreases over depth in the water column. This decrease becomes clear when comparing the sensitivity of Eqs. 1 and 2 to a change in $[CO_3^{2-}]$ (ocean acidification):

$$\frac{d\Delta[CO_3^{2-}]}{d[CO_3^{2-}]} = 1 \quad (3)$$

$$\frac{d\Omega}{d[CO_3^{2-}]} = \frac{1}{[CO_3^{2-}]_{sat}}. \quad (4)$$

Accordingly, a change in $[CO_3^{2-}]$ always results in the same amount of change in $\Delta[CO_3^{2-}]$, whereas for Ω the respective change depends on the ambient $[CO_3^{2-}]_{sat}$. Due to the increasing solubility of $CaCO_3$ ($[CO_3^{2-}]_{sat}$) with pressure, the sensitivity of Ω to $[CO_3^{2-}]$ is about half as strong at 3000 m depth as it would be at the surface (purple line in Fig. 1a), and even less (about one third) at the bottom. Differently spoken, the same amount of $[CO_3^{2-}]$ change has a larger impact on the value of Ω at the sea surface than it has at depth. This fact was already mentioned by Archer et al. (1989), who correctly concluded that it is negligible when considering equal pressure (depth) levels. However, across pressure gradients this effect leads to the artifact of an apparent decrease in the resulting acidification at greater depth, when using the change of Ω as measure for ocean acidification. The analysis clearly illustrates that both expressions ($\Delta[CO_3^{2-}]$, Ω) are not equally applicable for the assessment of ocean acidification over depth in the water column.

1.3 Relevance for the calculation of $CaCO_3$ dissolution kinetics

The definition of the sea water saturation state with respect to $CaCO_3$ is particularly important for the calculation of $CaCO_3$ dissolution from sinking and suspended parti-

BGD
10, 11343–11373, 2013

cles in the water column or from ocean sediments, which is defined as (Keir, 1980):

$$R_{CaCO_3} = CaCO_3 \cdot k \cdot S^n, \quad (5)$$

where k is the dissolution rate constant, transforming the degree of undersaturation (S) into a time dependent rate (R_{CaCO_3}) of particulate $CaCO_3$ that is being dissolved, and n is the reaction rate order, quantifying the degree of non-linearity of the dissolution reaction. The two constants (k, n) depend on each other and they need to be empirically determined (Gangstø, 2009), which is usually done in laboratory studies under atmospheric (sea surface) pressure conditions. Although $CaCO_3$ dissolution is probably not a first order (linear) function with respect to undersaturation (Keir, 1980), S is providing the thermodynamic gradient that is ultimately necessary to drive $CaCO_3$ dissolution.

Keeping in mind the different sensitivities of Ω and $\Delta[CO_3^{2-}]$ to ocean acidification (Eqs. 3 and 4), the use of Ω in the expression $S = (1 - \Omega)^n$ in Eq. (5) (Keir, 1980; Archer, 1991) has the counter-intuitive effect to result in an apparently slower deep ocean $CaCO_3$ dissolution in response to a $[CO_3^{2-}]$-change than it would be found at the sea surface for the same decrease in $[CO_3^{2-}]$, although the overall solubility ($[CO_3^{2-}]_{sat}$) is higher at depth. This paradox becomes even more pronounced when considering that reaction rate orders (n) may reach values up to 4.5 (Keir, 1980, 1983), such that the resulting dissolution at depth would be decelerated by a factor up to 100 (Fig. 1b). This value can be determined by relating the sensitivity of $(1\text{-}\Omega)^n$ (Keir, 1980; Archer, 1991) to $[CO_3^{2-}]$:

$$\frac{d(1-\Omega)^n}{d\left[CO_3^{2-}\right]} = \frac{-n \cdot \mathrm{abs}\left(\left[CO_3^{2-}\right]_{sat} - \left[CO_3^{2-}\right]\right)^{n-1}}{\left[CO_3^{2-}\right]_{sat}^{n}} \quad (6)$$

BGD
10, 11343–11373, 2013

at any depth (z) to the respective value at the sea surface (surf), which can be simplified as

$$\left(\frac{\left[CO_3^{2-}\right]_{\text{sat, surf}}}{\left[CO_3^{2-}\right]_{\text{sat},z}} \right)^n . \quad (7)$$

$CaCO_3$ dissolution has already been extensively studied (Morse and Berner, 1972, 2002; Berner and Morse, 1974; Keir, 1980, 1983; Hales and Emerson, 1997), and usually Eq. (2) is applied to describe the degree of (under-) saturation (Keir, 1980; Zeebe and Wolf-Gladrow, 2001). In a single field study, however, it was shown that for Aragonite dissolution at different pressure levels $\Delta[CO_3^{2-}]$ instead of Ω seems to be the more appropriate measure to represent the dissolution kinetics (Acker et al., 1987). Nevertheless, as both formulations will eventually result in the same amount of $CaCO_3$ being dissolved, they are usually considered as equally applicable, e.g. in ocean biogeochemical models including marine sediments that are used to calculate the attenuation time scale of buffering the anthropogenic CO_2 perturbation by $CaCO_3$ dissolution from sinking particles and especially ocean sediments (Archer, 1991).

2 Methods

2.1 Models

The present study comprises experiments with the ocean biogeochemical model PISCES (Aumont et al., 2003), which is driven by two different global ocean circulation fields. First, the PISCES model is forced off-line with 5-day averages of a circulation field obtained from the standalone ocean model OPA9.2 (Madec et al., 1998), which in turn uses the forcing detailed in Aumont and Bopp (2006). This model runs on the ORCA2.0 grid with a horizontal resolution of 2° × (0.5)–2° (longitude × latitude) and 31

BGD
10, 11343–11373, 2013

vertical levels. The layer thickness increases over depth from 10 m for the upper 10 levels to 500 m at depth, so that there are 12 levels in the upper 125 m. The resulting experiments are referred to as NEMO. Secondly, the PISCES model is included in the intermediate complexity Bern3D model (Müller et al., 2006), referred to as BERN. The Bern3D model has a horizontal resolution of 36 × 36 grid boxes (i.e. 10° × 5°) and 32 vertical levels. The layer thickness increases towards the ocean bottom starting with a thickness of 39 m (surface layer) and ending with a 397 m thick bottom layer. The first 125 m consist of three levels. The BERN model is forced with seasonal fields of temperature, salinity and wind stress. The seasonal forcing is based on monthly climatologies and thus the same from year to year. The standalone Bern3D model was first integrated over 10 000 yr with restoring boundary conditions on temperature and salinity. To provide mixed boundary conditions air-sea fresh water fluxes were diagnosed and averaged over 1000 yr after reaching the equilibrium. Finally mixed boundary conditions were applied with the prescribed fresh water fluxes and an additional fresh water flux correction in order to intensify the Atlantic meridional overturning circulation. The Bern3D model was then integrated over 5000 yr with mixed boundary conditions. Finally the Bern3D model and the PISCES model were coupled. A more detailed description of the forcing set up can be found in Gangstø et al. (2011). Consequently, two different (OPA9.2, Bern3D) fields of temperature and salinity, as well as resulting circulation fields are used to drive the ocean biogeochemical model PISCES. The circulation of OPA9.2 is described in more detail in Bordelon-Katrynski and Schneider (2012) and the Bern3D circulation in Müller et al. (2006, 2008).

The PISCES marine ecosystem model (Aumont and Bopp, 2006) simulates the biogeochemical cycling of dissolved inorganic carbon (DIC), oxygen (O_2), and total alkalinity (TALK) and the main nutrients phosphate (PO_4), nitrate (NO_3), ammonium (NH_4), silicate ($SiOH_4$), and iron (Fe), which control biological productivity. The model includes two phytoplankton size classes (big and small), representing nanophytoplankton and diatoms and two zooplankton size classes (big and small) for micro- and mesozooplankton. There are three non-living organic carbon components, which are dissolved

BGD
10, 11343–11373, 2013

organic matter (DOM), and small and big sinking particles (POM). Calcification is realized via grazing and mortality of nanophytoplankton, both dependent on temperature and nutrient availability. During grazing 85 % of the $CaCO_3$ ingested is assumed to pass the guts of the grazers. This share represents the net calcification and affects DIC and TALK (sink) and the pool of particulate $CaCO_3$ pool (source) (Aumont and Bopp, 2006; Gangstø et al., 2011). The sinking speed of particulate matter is prescribed in the PISCES model. In NEMO small organic carbon particles sink at a rate of $3\,m\,d^{-1}$, whereas particles of the large size class (POC, $CaCO_3$, Opal) start with a sinking speed of $50\,m\,d^{-1}$ in the mixed layer and accelerate up to $250\,m\,d^{-1}$ at greater depth. In the BERN model all particles sink with constant velocities. Small organic carbon particles sink with $3\,m\,d^{-1}$, while large particles (POC, $CaCO_3$, Opal) sink with $60\,m\,d^{-1}$ (Gangstø et al., 2011). As all detrital particles are treated to sink individually in PISCES, a potential impact of mineral ballasting on the sinking speed of particles is not considered in this study.

2.2 Parameterization of $CaCO_3$ dissolution

As it was mentioned above, for the kinetic expression of $CaCO_3$ dissolution according to Eq. (5), the dissolution rate constant k has to be empirically determined. Therefore, in the present study a sediment trap data set including stations with annually averaged particulate $CaCO_3$ fluxes from at least two deployment depths at the same location is used (Dittert et al., 2005). To calculate the calcite dissolution rate from the difference between the fluxes at two depths, the calcite concentrations and the particle residence time between two depths need to be known. For this purpose the sinking speed of $CaCO_3$ particles (corresponding to the sinking speed of large POM) from the model is used. To consider the $CaCO_3$ saturation state of the ambient seawater (S in Eq. 5) the water column between two deployment depths is divided into layers of 200 m vertical extent, so that in combination with data from the GLODAP data base (Key et al., 2004) a residence-time weighted mean $CaCO_3$ saturation value (Ω, $\Delta[CO_3^{2-}]$) can be

BGD
10, 11343–11373, 2013

calculated for each sediment trap location. Finally, the dissolution rate constant k is optimized by minimizing the root mean square error between theoretical calcite dissolution (using the same k in Eq. (5) for all sediment trap stations) and the respective observed dissolution values. For the theoretical dissolution the degree of undersaturation S is either given by Ω or $\Delta[CO_3^{2-}]$, while for the reaction rate order n three different values (1, 2, 4.5) are chosen to cover the range of n as given in the literature (Keir, 1980). An overview of the resulting six combinations of reaction rate orders and the empirically determined dissolution constants k is given in Table 1. Generally, the value of k increases with the degree of non-linearity (n) of the kinetic expression, because higher order expressions are less sensitive to low values of undersaturation.

2.3 Experiments

Both models were first spun up with their standard expression of calcite dissolution (Ω, $n = 1$) for several thousands of years under constant atmospheric CO_2 to reach equilibrium. In particular, NEMO was initialized with GLODAP data (Key et al., 2004) for DIC and TALK and a CO_2 of 286 ppm. The BERN model was initialized with a global mean alkalinity between the global average from GLODAP (Key et al., 2004) and the one from Goyet et al. (2000), using an atmospheric CO_2 of 278 ppm.

In order to compare the effect of different possible kinetic expressions of calcite dissolution six experiments were carried out for each model. According to the expression of undersaturation S (either as Ω or as $\Delta[CO_3^{2-}]$) and the reaction rate order n (1, 2 or 4.5) these are named $\Omega 1$, $\Omega 2$, $\Omega 4.5$, $\Delta 1$, $\Delta 2$, and $\Delta 4.5$, respectively (see also Table 1). These experiments were started from the respective spinups mentioned above and integrated over 3000 yr each to reach steady state.

In a next step, to test the sensitivity of the different kinetic expressions to ocean acidification the six experiments explained above were forced by an atmospheric CO_2 scenario prescribing an increase at a rate of 1 % CO_2 per year. This increase was applied over 140 yr until 4× preindustrial CO_2 was reached (BERN: 1120 ppm and NEMO: 1151 ppm). Afterwards CO_2 was kept constant at this value while the scenarios were

BGD
10, 11343–11373, 2013

continued until they reached 1000 yr of integration. These transient experiments were started from the equilibrium runs after 3000 yr. The equilibrium runs were continued for 1000 yr to serve as control simulations for the respective scenarios. Please note that the climate and ocean circulation are not affected by the CO_2 scenario, staying in preindustrial state. Furthermore, neither cycling of organic carbon and nutrients nor calcification are sensitive to ocean acidification.

3 Results and discussion

3.1 Steady state

The spatial agreement of the steady state model results with observation based estimates is shown in a taylor diagram for the variables total alkalinity (TALK), dissolved inorganic carbon (DIC), calcite saturation horizon (CSH), saturation state (Ω and $\Delta[CO_3^{2-}]$), and apparent oxygen utilization (AOU), displaying the pattern correlation coefficients and normalized standard deviations (Taylor, 2001). A perfect model run would reside at the intercept, with a normalized standard deviation of 1.0 and a correlation coefficient of 1.0 (Fig. 2). First of all, it becomes clear that for all carbonate system variables the respective distributions differ between the experiments as a result of the varied calcite dissolution kinetics. This result shows that different ways to parameterize calcite dissolution are not equally applicable. As expected, and used as a consistency check, the AOU values do not change between the different parameterizations, but only between the two models used. For both models the best match between model results and observations is found for the distributions of both Ω and $\Delta[CO_3^{2-}]$. Both variables are almost equally well reproduced with slightly too high normalized standard deviations (values above one) by both models. The depth of the CSH serves as a further (2-dimensional) measure of the seawater $CaCO_3$ saturation. It is distinctly less well reproduced by both models (NEMO: $R = 0.84$, BERN: $R = 0.45$) than Ω and $\Delta[CO_3^{2-}]$ including too little spatial variability.

BGD
10, 11343–11373, 2013

Interestingly, although the amount of particulate $CaCO_3$ in the water column and consequently its annual dissolution rate is a small number compared to the high background concentrations of DIC and TALK, both variables show significant variations among the different experiments, as can be seen in the Taylor diagram (Fig. 2). While overestimating spatial variability of both variables in both models, DIC is generally better reproduced than TALK. For the latter the BERN model has a better spatial correlation ($R \sim 0.9$) than NEMO ($R \sim 0.8$). Unfortunately, none of the model realizations sticks out as clearly the best and could therefore serve as proof-of-concept for the most plausible kinetic description of calcite dissolution. Consequently, other factors such as calcite formation (Gehlen et al., 2007), formation and dissolution of aragonite (Gangstø et al., 2008) and ocean circulation will also play a role. However, the variations in the spatial distribution of DIC and TALK can be straightforwardly explained by the different dissolution kinetics, in particular by the formulation of the degree of undersaturation (S) and the reaction rate order (n), as outlined below.

3.1.1 Impact of the reaction rate order (n) on the distribution of DIC and TALK

The vertical gradient of TALK serves as an indicator of the efficiency of the $CaCO_3$ counter pump (Heinze et al., 1991). As expected and shown by all simulations in the present study, the higher the vertical TALK gradient, for example given by the difference between the top 100 m of the water column and 3700 m depth, the lower the total inorganic carbon (DIC) inventory in the ocean (Table 2). This results from the low surface TALK concentrations causing a low buffer (uptake) capacity for CO_2 from the atmosphere. Both models simulate higher vertical TALK gradients than given by the GLODAP data (Key et al., 2004), while BERN has a higher and NEMO a lower DIC inventory than given by GLODAP. In both models the overestimation of the TALK gradients is caused by too low surface TALK concentrations (not shown), which may be an indicator for the neglect of shallow aragonite cycling (Gangstø et al., 2008). In addition to this, the deviation from the GLODAP data may also result from different temperature and salinity distributions as well as circulation fields (solubility pump) and it is also likely

BGD
10, 11343–11373, 2013

that they are affected by differences in the vertical flux of organic carbon (soft tissue pump) (Volk and Hoffert, 1985).

With an increasing reaction rate order (n) there is a systematic increase of the vertical TALK gradient across all experiments, equally caused by TALK decreasing at the surface and increasing at depth. As mentioned above, this stronger separation can be explained with a reduced sensitivity of calcite dissolution to low values of $CaCO_3$ undersaturation in kinetic expressions with higher reaction rate orders. In order to yield the same amount of calcite dissolution, a stronger degree of undersaturation is needed under a higher n. This effect is shown by decreasing dissolution weighted Ω values and more negative $\Delta[CO_3^{2-}]$ at higher rate orders (Table 2). Consequently, calcite is preferentially dissolving in deeper layers when reaction rate orders are higher. Following the deeper calcite dissolution, particles spend less time at effectively undersaturated conditions, so that the total calcite dissolution is also slightly reduced under higher reaction rate orders (Table 2).

The impact of the reaction rate order on the vertical TALK gradient also influences the tilt of the CSH, which is usually lying deep in the North Atlantic and shoaling along the conveyor belt circulation pathway towards the North Pacific and northern Indian Ocean. The preferential deep calcite dissolution under higher reaction rate orders therefore causes a stronger tilt of the CSH, which means it moves deeper in the North Atlantic and shoals in the North Pacific (not shown).

3.1.2 Impact of the formulation of $CaCO_3$ saturation (S) on the distribution of TALK (Ω vs. $\Delta[CO_3^{2-}]$)

The effect of the different descriptions of undersaturation (S) can also be depicted when regarding the vertical gradient of TALK. Both models show a slightly increased gradient for the experiments using $\Delta[CO_3^{2-}]$ in contrast to those using Ω. This means that at equal reaction rate orders n the Ω formulation has a tendency to dissolve calcite at shallower depths. This effect is in line with the reduced sensitivity of Ω based dissolution at greater depth as it was demonstrated in Sect. 1.2. For our simulations

BGD
10, 11343–11373, 2013

a stronger shallow calcite dissolution when using Ω instead of $\Delta[CO_3^{2-}]$ is explained by the fact that the optimization of the dissolution rate constant k in our study is centered around a depth of about 3000 m, which is due to the deployment depths of the sediment traps. While in the sensitivity study (Sect. 1.2) the sensitivity of Ω at every depth was related to the sea surface, the centering of the optimization of k around 3000 m depth is expected to yield a higher (lower) sensitivity for Ω than for Δ expressions at shallower (greater) depths. In fact, both expressions (Ω, $\Delta[CO_3^{2-}]$) yield the same amount of calcite dissolution in the depth range of 2000–4000 m for all reaction rate orders. In contrast to this, and as it can be expected from the sensitivity analysis in Sect. 1.2, the Ω experiments simulate a total calcite dissolution which is 20 % and 12 % (BERN, NEMO) higher than in the Δ experiments for the upper 2000 m when using $n = 1$. This increased sensitivity further amplifies under a higher reaction rate order, so that for $n = 4.5$ the Ω formulation reaches a dissolution rate which is 103 % and 173 % (BERN, NEMO) higher than when using Δ. In line with this vertical sensitivity gradient of the Ω formulation, there is a 3 % and 7 % (BERN, NEMO) lower calcite dissolution compared to Δ below 4000 m water depth.

3.1.3 Model differences (BERN vs. NEMO)

The two models that are used in the present study mostly differ in the physical forcing that is applied to the biogeochemical model PISCES, which means in the variables temperature, salinity and the velocity field. This causes differences in the transport of carbon and nutrients, which in turn affects patterns of primary production and thus calcification. Furthermore, both models also differ in the treatment of particle sinking speeds (see model description). Since the aim of this study is a systematic investigation of the effects of varying kinetic expressions for calcite dissolution, we will refrain from a deeper analysis on the realism of productivity, calcification and nutrient fields in each model. Instead, we will focus in this section on effects arising from the circulation fields and different particle sinking speeds.

BGD
10, 11343–11373, 2013

Generally, both models show some indications of weak deep ventilation. In the BERN model this is manifested by an overestimation of the AOU, which amounts on global average to 200 $\mu mol\,L^{-1}$ (NEMO: 134 $\mu mol\,L^{-1}$) in contrast to 157 $\mu mol\,L^{-1}$ from the world ocean atlas (Collier and Durack, 2006). Interestingly, both models exhibit about the same average oxygen consumption per gigaton carbon of primary production (PP; BERN: 46 $Gt\,C\,yr^{-1}$; NEMO: 33 $Gt\,C\,yr^{-1}$), which amounts to approximately 4.2 $\mu mol\,L^{-1}\,(Gt\,C)^{-1}$, and furthermore, both models agree on a scaling factor between PP and the Atlantic Meridional Overturning Circulation (AMOC; BERN: 22 Sv; NEMO: 16 Sv) with a ratio of 2.1 $Gt\,C\,yr^{-1}\,Sv^{-1}$. As a consequence, the AOU also positively scales with the overturning, which is a counterintuitive result, since one would expect a stronger downward transport of oxygen, and thus reduced AOU, with a more vigorous AMOC. Most probably, this offset occurs due to the effect that PP rapidly responds to nutrient upwelling and mixing into the sunlit shallow ocean, maybe even below the layers that are in direct contact with the atmosphere. In contrast, for oxygen water masses need to remain sufficiently long in the surface mixed layer to effectively equilibrate with the atmosphere and then be able to subduct with a considerable amount of replenished oxygen.

In the NEMO model sluggish deep ventilation is shown by a 15 % overestimation of the volume of calcite-undersaturated water masses, mostly at the expense of slightly oversaturated water masses ($1 < \Omega < 2$; Fig. 3). This overestimation is especially large for the most acidic water masses. In the BERN model the distribution between over- and undersaturated waters corresponds very well with the data, and the volume of the most undersaturated areas is only slightly overestimated. In both models the volume of highly undersaturated water masses decreases with higher reaction rate orders. This effect can be explained by the tendency of the high rate order simulations to preferentially dissolve the calcite at greater depth, as indicated by the dissolution weighted values of Ω and Δ (Table 2). The fact that the volumes of the most undersaturated water masses are much better reproduced by the BERN model will be caused by the effect that, although both models produce the same amount of cal-

BGD
10, 11343–11373, 2013

cite (1.1 Gt $CaCO_3$ yr^{-1}), BERN more efficiently dissolves the calcite at global scale (BERN$\sim$ 0.4 Gt yr^{-1}; NEMO $\sim$ 0.1 Gt yr^{-1}). This more efficient dissolution is most probably driven by the lower prescribed sinking speeds in the BERN model, allowing a longer residence time of the calcite particles in the deep ocean where undersaturation is high.

3.2 Transient Simulations

The atmospheric CO_2 scenario applied prescribes the CO_2 to increase from preindustrial values to 1120 ppm (BERN) and 1151 ppm (NEMO) after 140 yr, staying constant at these values, afterwards. As a result of ocean acidification global calcite dissolution increases strongly in all experiments (Fig. 4, Table 2). In NEMO the relative dissolution, i.e. the fraction of dissolution relative to net production, is almost doubled from 9 to 16 %, whereas in BERN there is almost complete dissolution reached ($\sim$ 98 %; before: 36 %).

Due to the gradual propagation of the CO_2 perturbation from the surface towards greater depth, calcite dissolution first responds with a slight increase at intermediate depths (2000–4000 m), where water masses are the first to switch from over- to undersaturation. From about the year 100 on shallow calcite dissolution starts to strongly increase in both models and all experiments (0–2000 m), while at intermediate and greater depths (below 4000 m) dissolution strongly declines, so that eventually the overall increase in global calcite dissolution occurs in the upper ocean. This shift is caused by the massive CO_2 uptake through the ocean surface and relatively high calcite particle concentrations at shallower depths. As a consequence of this shallow calcite dissolution (Fig. 4) there is a drop in the flux of calcite into the deep ocean (Fig. 5), which will be explained in more detail, below.

The shift in the depth distribution of calcite dissolution causes a reorganization of the vertical TALK gradient, with an accumulation of TALK near the surface and a depletion at greater depth (Table 2). Until year 140 this gradient reduces in all simulations, while it almost disappears in the BERN model and even reverses in NEMO in year 1000

BGD
10, 11343–11373, 2013

(Table 2). The uptake of anthropogenic CO_2 is very similar in all simulations until year 140 with a higher uptake in BERN than in NEMO. Until year 1000 CO_2 uptake further increases but now the higher rate order experiments of the Δ series exhibit significantly less uptake than all other experiments in both models. This difference can again be explained by the generally higher sensitivity of Ω in contrast to Δ at shallow depth, which is even amplified under higher rate orders, as it was mentioned above.

With regard to the distribution of the over- and undersaturated water masses, both models predict a disappearance of water masses with $\Omega > 3$ until year 140 (Fig. 3). The fraction of undersaturated water masses expands to approximately 60 % in NEMO and 45 % in BERN. Apart from the differences between the models, i.e. generally larger undersaturated areas in NEMO than in BERN and less strongly undersaturated volumes with higher rate orders, the distribution remains similar to what is found for the steady state. In contrast to this, in the year 1000 both models predict very similar distributions of mostly undersaturated conditions. At this point about 85 % of the ocean is predicted to have saturation values of $\Omega < 0.8$ and there are neither differences between the formulation of undersaturation (Ω, Δ) nor the reaction rate order (n). This result shows that while during the first 140 yr an effect of the different calcite dissolution kinetics is still detectable in the distribution of the calcite saturation state, on longer term atmospheric CO_2 concentrations around 1000 ppm induce a strong ocean acidification signal, especially on the upper part of the water column, with devastating impact on calcite particles in the water column.

The latter can be clearly tracked when regarding the time series of the globally integrated particle fluxes across different depth levels. Close to the sea surface, where still the highest saturation values are yielded, calcite fluxes decrease in the NEMO model, depending on the kinetic expression applied. For most expressions the reduction stabilizes at about −2 %, which means there is only a negligible effect, whereas for the Ω4.5 expression the calcite export shows a 10 % reduction in year 1000, while it is still linearly decreasing (Fig. 5b). In the BERN model calcite export at 100 m remains virtually unaffected (Fig. 5a). In 1000 m water depth calcite fluxes of the different ex-

BGD
10, 11343–11373, 2013

periments have about the same initial values in each model and begin to decrease around year 100 (Fig. 5c, d), when shallow particle dissolution kicks in (Fig. 4). In this depth range the various kinetic expressions result in rather different rates of flux attenuation (BERN: −75 % to −91 %; NEMO: −56 % to −90 %). Generally, the Ω kinetics respond more quickly than the Δ expressions. In the NEMO model higher reaction rate orders have a tendency towards lower response when using Δ. At 3000 m depth, in contrast, all simulations start from different initial calcite fluxes, which results from the different sensitivities of the kinetic expressions to the initial saturation state distribution (see sensitivity analysis above). However, from about year 400 onward, the calcite fluxes at 3000 m depth have ceased (Fig. 5e, f) in all simulations, due to the massive acidification of the water column above.

The results of the transient experiments show that different kinetic expressions of calcite dissolution indeed have different sensitivities to ocean acidification. Apart from the devastating effect of ocean acidification, shown by the shut-down of calcite fluxes at 3000 m until about year 400, calcite fluxes at shallower depths (e.g. 1000 m) are clearly fanning out, depending on the kinetic expression applied. Although not considered in the present study, calcite is known to be an important ballast material for the sinking of organic carbon and nutrients (Armstrong et al., 2002; Klaas and Archer, 2002). Consequently, the large range of potential calcite flux attenuation at shallow to intermediate depth implies a strongly differential impact on the oceanic sink or anthropogenic CO_2.

4 Summary and conclusions

We test a range of plausible parameterizations for the kinetic expression of $CaCO_3$ dissolution in two ocean biogeochemical models, that explicitly link $CaCO_3$ dissolution to the degree of undersaturation of sea water with respect to $CaCO_3$. Although for steady state experiments differences in the fields of dissolved properties, especially alkalinity, are found, no parameterization stands out as clearly the best. This suggests that uncertainties in the parameterization of calcite production and/or aragonite cycling next to

BGD
10, 11343–11373, 2013

potential circulation deficits may also play an important role. All diagnosed differences in the distribution of alkalinity can be qualitatively and straightforwardly explained from the expected effects arising from the use of either Ω or Δ and the accompanying reaction rate orders (sensitivity study).

With regard to anthropogenic perturbations we show that proceeding ocean acidification causes a switch from deep calcite dissolution (at present) to rather shallow dissolution under high CO_2. Notably, a wide range of sensitivities, e.g. with regard to $CaCO_3$ flux at shallow and intermediate depths develops depending on the kinetic expression applied. Since calcite is an important mineral for particle ballasting (Armstrong et al., 2002; Klaas and Archer, 2002), its potential fate under ocean acidification is presently of high scientific interest (Gehlen et al., 2007; Gangstø, 2009; Gangstø et al., 2011). Based on our findings, different calcite dissolution kinetics may yield very different responses to ocean acidification and thereby influence the downward transport of organic carbon and nutrients in a wide range. Generally, particle ballasting is expected to be reduced, followed by a decline of organic carbon export. However, the impact on the ocean carbon sink and potentially resulting climate feedbacks is still an open question.

Calcite dissolution in the water column has proven to be a sufficiently fast process, allowing different kinetic expressions to leave an imprint on the distribution of alkalinity in a preindustrial ocean. On the other hand, it is slow enough that even under an aggressive ocean acidification scenario different flux patterns into the ocean interior towards intermediate depths occur with potential impacts on particle ballasting, as explained above. It remains to be investigated how different kinetic expressions would affect the dissolution of calcite from ocean sediments, which are known to provide an important further buffer to increase the uptake of anthropogenic CO_2 by the ocean (Archer, 1991). We can only speculate that if bottom water ventilation is a relatively slow process, so that (anthropogenically) acidified water masses can easily saturate, the kinetic expression will be of minor importance. However, if ventilation is rather fast and saturation of bottom water will not be reached, the different kinetic expressions may play an important role in the buffering time scale of the anthropogenic CO_2 per-

BGD
10, 11343–11373, 2013

turbation. Consequently, our results clearly show the need to better understand the factors driving calcite dissolution both in the water column and in ocean sediments to assess the strength and time scales of expected climate feedbacks.

Acknowledgements. This work was funded by the Cluster of Excellence Future Ocean (EXC80/1) and the Federal Ministry of Education and Research (BMBF, FKZ 03F0655M). We would like to thank Guy Munhoven for intensive discussion.

References

Acker, J. G., Byrne, R. H., Ben-Yaakov, S., R. A., F., and Betzer, P. R.: The effect of pressure on aragonite dissolution rates in seawater, Geochim. Cosmochim. Ac., 51, 2171–2175, 1987. 11349

Archer, D. E.: Equatorial Pacific calcite preservation cycles: production or dissolution?, Paleoceanography, 6, 561–571, doi:10.1029/91PA01630, 1991. 11348, 11349, 11361

Archer, D. E.: A data-driven model of the global calcite lysocline, Global Biogeochem. Cy., 10, 511–526, 1996. 11346

Archer, D. E.: Fate of fossil fuel CO_2 in geologic time, J. Geophys. Res., 110, doi:10.1029/2004JC002625, 2005. 11345

Archer, D. E., Emerson, S., and Reimers, C.: Dissolution of calcite in deep-sea sediments: pH and O_2 microelectrode results, Geochim. Cosmochim. Ac., 53, 2831–2845, 1989. 11347

Armstrong, R. A., Lee, C., Hedges, J. I., Honjo, S., and Wakeham, S. G.: A new, mechanistic model for organic carbon fluxes in the ocean based on the quantitative association of POC with ballast minerals, Deep-Sea Res. Pt. II, 49, 219–236, 2002. 11360, 11361

Aumont, O. and Bopp, L.: Globalizing results from ocean in situ iron fertilization studies, Global Biogeochem. Cy., 20, GB2017, doi:10.1029/2005GB002591, 2006. 11349, 11350, 11351

Aumont, O., Maier-Reimer, E., Blain, S., and Monfray, P.: An ecosystem model of the global ocean including Fe, Si, P colimitations, Global Biogeochem. Cy., 17, 1060, doi:10.1029/2001GB001745, 2003. 11349

Bach, L. T., Bauke, C., Meier, K. J. S., Riebesell, U., and Schulz, K. G.: Influence of changing carbonate chemistry on morphology and weight of coccoliths formed by *Emiliania huxleyi*, Biogeosciences, 9, 3449–3463, doi:10.5194/bg-9-3449-2012, 2012. 11345

BGD
10, 11343–11373, 2013

Barker, S., Higgins, J. A., and Elderfield, H.: The future of the carbon cycle: review, calcification response, ballast and feedback on atmospheric CO_2, Philos. T. R. Soc. London A, 361, 1977–1999, doi:10.1098/rsta.2003.1238, 2003. 11345

Berner, R. A. and Morse, J. W.: Dissolution kinetics of calcium carbonate in sea water; IV, Theory of calcite dissolution, Am. J. Sci., 274, 108–134, doi:10.2475/ajs.274.2.108, 1974. 11349

Bordelon-Katrynski, L. A. and Schneider, B.: Feedbacks of CO_2 dependent dissolved organic carbon production on atmospheric CO_2 in an ocean biogeochemical model, Biogeosciences Discuss., 9, 7983–8011, doi:10.5194/bgd-9-7983-2012, 2012. 11350

Caldeira, K. and Wickett, M. E.: Anthropogenic carbon and ocean pH, Nature, 425, p. 365, doi:10.1073/pnas.0702737104, 2003. 11345

Canadell, J. G., Quéré, C. L., Raupach, M. R., Field, C. B., Buitenhuis, E. T., Ciais, P., Conway, T. J., Gillett, N. P., Houghton, R. A.,, and Marland, G.: Contributions to accelerating atmospheric CO_2 growth from economic activity, carbon intensity, and efficiency of natural sinks, P. Natl. Acad. Sci. USA, 104, 18866–18870, doi:10.1073/pnas.0702737104, 2007. 11344

Collier, M. A. and Durack, P. J.: CSIRO netCDF version of the NODC World Ocean Atlas 2005, 1–45, CSIRO, Victoria, Australia, 2006. 11357

Dittert, N., Corrin, L., Bakker, D., Bendsen, J., Gehlen, M., Heinze, C., Maier-Reimer, E., Michalopoulus, P., Soetaert, K. E. R., and Tol, R. J.: Integrated data sets of the FP5 Research Project ORFOIS: origin and fate of biogenic particle fluxes in the ocean and their interactions with atmospheric CO_2 concentrations as well as the marine sediment, WDC-MARE Reports 0002, vol. 1, Alfred Wegener Institute for Polar and Marine Research and MARUM, Bremerhaven, Bremen, 2005. 11351

Fabry, V. J., Seibel, B. A., Feely, R. A., and Orr, J. C.: Impacts of ocean acidification on marine fauna and ecosystem processes, ICES J. Mar. Sci., 65, 414–432, doi:10.1093/icesjms/fsn048, 2008. 11345

Feely, R. A., Sabine, C. L., Lee, K., Berelson, W., Kleypas, J., Fabry, V. J., and Millero, F. J.: Impact of anthropogenic CO_2 on the $CaCO_3$ system in the oceans, Science, 305, 362–366, doi:10.1126/science.1097329, 2004. 11346

Gangstø, R.: Increasing atmospheric CO_2, ocean acidification and pelagic ecosystems, Ph. D. thesis, Physikalisches Institut der Universität Bern, 2009. 11348, 11361

BGD
10, 11343–11373, 2013

Gangstø, R., Gehlen, M., Schneider, B., Bopp, L., Aumont, O., and Joos, F.: Modeling the marine aragonite cycle: changes under rising carbon dioxide and its role in shallow water $CaCO_3$ dissolution, Biogeosciences, 5, 1057–1072, doi:10.5194/bg-5-1057-2008, 2008. 11354

Gangstø, R., Joos, F., and Gehlen, M.: Sensitivity of pelagic calcification to ocean acidification, Biogeosciences, 8, 433–458, doi:10.5194/bg-8-433-2011, 2011. 11345, 11350, 11351, 11361

Gehlen, M., Gangstø, R., Schneider, B., Bopp, L., Aumont, O., and Ethe, C.: The fate of pelagic $CaCO_3$ production in a high CO_2 ocean: a model study, Biogeosciences, 4, 505–519, doi:10.5194/bg-4-505-2007, 2007. 11346, 11354, 11361

Gehlen, M., Bopp, L., and Aumont, O.: Short-term dissolution response of pelagic carbonate sediments to the invasion of anthropogenic CO_2: a model study, Geochem. Geophy. Geosy., 9, Q02012, doi:10.1029/2007GC001756, 2008. 11346

Goyet, C., Healy, R. J., and Ryan, J. P.: Global Distribution of Total Inorganic Carbon and Total Alkalinity Below the Deepest Winter Mixed Layer Depths, Carbon Dioxide Information Analysis Center, Oak Ridge National Laboratory, US Department of Energy, Tennessee, Oak Ridge, 2000. 11352

Hales, B. and Emerson, S.: Evidence in support of first-order dissolution kinetics of calcite in seawater, Earth Planet. Sc. Lett., 248, 317–327, 1997. 11349

Heinze, C., Maier-Reimer, E., and Winn, K.: Glacial pCO_2 reduction by the World Ocean: experiments with the Hamburg Carbon Cycle Model, Paleoceanography, 6, 395–430, 1991. 11354

Hofmann, M. and Schnellnhuber, H.-J.: Impacts of ocean acidification on marine fauna and ecosystem processes, P. Natl. Acad. Sci. USA, 106, 3017–3022, doi:10.1073/pnas.0813384106, 2009. 11345

Iglesias-Rodriguez, M. D., Halloran, P. R., Colmenero-Hidalgo, E., Gittins, J. R., Green, D. R. H., Tyrrell, T., Gibbs, S. J., von Dassow, P., Rehm, E., Armbrust, E. V., and Boessenkool, K. P.: Phytoplankton calcification in a high-CO_2 world, Science, 320, 336–340, 2008. 11345

Keir, R.: The dissolution kinetics of biogenic calcium carbonates in seawater, Geochim. Cosmochim. Ac., 44, 241–252, 1980. 11348, 11349, 11352

Keir, R.: Variation in the carbonate reactivity of deep-sea sediments: determination from flux experiments, Deep-Sea Res., 30, 279–296, 1983. 11348, 11349

Key, R. M., Kozyr, A., Sabine, C. L., Lee, K., Wanninkhof, R., Bullister, J. L., Feely, R. A., Millero, F. J., Mordy, C., and Peng, T.-H.: A global ocean carbon climatology: re-

BGD
10, 11343–11373, 2013

sults from Global Data Analysis Project (GLODAP), Global Biogeochem. Cy., 18, doi:10.1029/2004GB002247, 2004. 11345, 11351, 11352, 11354, 11368, 11369, 11370, 11371

Klaas, C. and Archer, D. E.: Association of sinking organic matter with various types of mineral ballast in the deep sea: implications for the rain ratio, Global Biogeochem. Cy., 16, 1116, doi:10.1029/2001GB001765, 2002. 11360, 11361

Kleypas, J. A., Feely, R. A., Fabry, V. J., Langdon, C., Sabine, C. L., and Robbins, L. L.: Impacts of Ocean Acidification on Coral Reefs and on other Marine Calcifiers: A Guide for Future Research, sponsored by NSF, NOAA, and the US Geological Survey, St. Petersburg, 88 pp., www.isse.ucar.edu/florida/, 2006. 11345

Langer, G., Geisen, M., Baumann, K., Kläs, J., Riebesell, U., Thoms, S., and Young, J. R.: Species-specific responses of calcifying algae to changing seawater carbonate chemistry, Geochem. Geophy. Geosy., 7, Q09006, doi:10.29/2005GC001227, 2006. 11345

Lohbeck, K. T., Riebesell, U., and Reusch, T. B. H.: Adaptive evolution of a key phytoplankton species to ocean acidification, Nat. Geosci., 5, 346–351, doi:10.1038/ngeo1441, 2012. 11345

Madec, G., Delecluse, P., Imbard, M., and Lévy, C.: OPA 8.1 Ocean General Circulation Model Reference Manual, Tech. Rep. 11, IPSL, 1998. 11349

Morse, J. W. and Berner, R. A.: Dissolution kinetics of calcium carbonate in sea water: II. A kinetic origin for the lysocline, Am. J. Sci., 272, 840–851, 1972. 11349

Morse, J. and Berner, R.: The dissolution kinetics of major sedimentary carbonate minerals, Earth-Sci. Rev., 59, 51–84, 2002. 11349

Müller, S. A., Joos, F., Edwards, N. R., and Stocker, T. F.: Water mass distribution and ventilation time scales in a cost-efficient, three-dimensional ocean model, J. Climate, 19, 5479–5499, 2006. 11350

Müller, S. A., Joos, F., Plattner, G.-K., Edwards, N. R., and Stocker, T. F.: Modeled natural and excess radiocarbon: sensitivities to the gas exchange formulation and ocean transport strength, Global Biogeochem. Cy., 22, GB3011, doi:10.1029/2007GB003065, 2008. 11350

Riebesell, U.: Reduced calcification of marine plankton in response to increased atmospheric CO_2, Nature, 407, 364–367, 2000. 11345

Sabine, C. L., Feely, R. A., Gruber, N., Key, R. M., Lee, K., Bullister, J. L., Wanninkhof, R., Wong, C. S., Wallace, D. W. R., Tilbrook B., Millero, F. J., Peng, T.-H., Kozyr, A., Ono,

BGD
10, 11343–11373, 2013

T., and Rios, A. F.: The oceanic sink for anthropogenic CO_2, Science, 305, 367–371, doi:10.1126/science.1097403, 2004. 11346
Schiebel, R.: Planktic foraminiferal sedimentation and the marine calcite budget, Global Biogeochem. Cy., 16, 1065, doi:10.1029/2001GB001459, 2002. 11345
Sundquist, E. T.: Influence of deep-sea benthic processes on atmospheric CO_2, Philos. T. Roy. Soc. London, 331, 155–165, doi:10.1098/rsta.1990.0062, 1990. 11345
Takahashi, T., Sutherland, S. C., Wanninkhof, R., Sweeney, C., Feely, R. A., Chipman, D. W., Hales, B., Friederich, G., Chavez, F., Sabine, C., Watson, A., Bakker, D. C., Schuster, U., Metzl, N., Yoshikawa-Inoue, H., Ishii, M., Midorikawa, T., Nojiri, Y., Körtzinger, A., Steinhoff, T., Hoppema, M., Olafsson, J., Arnarson, T. S., Tilbrook, B., Johannessen, T., Olsen, A., Bellerby, R., Wong, C., Delille, B., Bates, N., and de Baar, H. J.: Climatological mean and decadal change in surface ocean pCO_2, and net seaair CO_2 flux over the global oceans, Deep-Sea Res. Pt. II, 56, 554–577, doi:10.1016/j.dsr2.2008.12.009, 2009. 11370
Taylor, K. E.: Summarizing multiple aspects of model performance in a single diagram, J. Geophys. Res., 106, 7183–7192, 2001. 11353
Volk, T. and Hoffert, M. I.: Ocean carbon pumps: Analysis of relative strengths and efficiencies in ocean-driven atmospheric CO_2 changes, in: The Carbon Cycle and Atmospheric CO_2: Natural Variations Archean to Present, edited by: Sundquist, E., and Broecker, W. S., vol. 32 of Geophysical Monograph Series, AGU, Washington DC, 99–110, 1985. 11355
Zeebe, R. E. and Wolf-Gladrow, D.: CO_2 in Seawater: Equilibrium, kinetics, isotopes, Elsevier Oceanography Series 65, 346 pp., 2001. 11345, 11347, 11349

BGD
10, 11343–11373, 2013

Table 1. Optimized dissolution rate constant k [d^{-1}] as function of reaction rate order n determined for the Ω and Δ formulations.

$S\backslash n$	1	2	4.5
Ω	3.4	20.0	1729
Δ	3.6	22.5	3288

BGD
10, 11343–11373, 2013

Table 2. Diagnostics of the marine carbonate system for the different models (N, B) and experiments and GLODAP data (G) (Key et al., 2004). Shown are the vertical gradient of TALK (3700 m – surface 100 m), global DIC/anthropogenic carbon (C_{anth}) inventory, dissolution-weighted saturation value either based on Ω or $\Delta[CO_3^{2-}]$ and total calcite dissolution. The results are shown for (a) steady state; (b) after quadrupling CO_2 (year 140), and (c) after stabilization (year 1000).

	Source	Ω1	Ω2	Ω4.5	Δ1	Δ2	Δ4.5
(a) steady state							
TALK grad. [µmol L^{-1}]	N	103.2	109.2	116.9	107.3	116.6	132.0
	B	112.0	116.2	116.6	113.4	120.4	121.0
	G	75.2					
DIC inv. [Gt C]	N	34 086	34 077	34 068	34 080	34 067	34 042
	B	36 710	36 698	36 694	36 707	36 690	36 686
	G	35 969					
diss. weighted saturation	N	0.87	0.85	0.82	−11.22	−13.94	−16.57
	B	0.91	0.89	0.86	−5.70	−10.32	−12.74
total diss. [Gt yr^{-1}]	N	0.11	0.11	0.10	0.11	0.10	0.10
	B	0.40	0.36	0.36	0.39	0.35	0.36
(b) 140 yr							
TALK grad. [µmol L^{-1}]	N	98.0	104.6	112.7	103.3	113.8	130.2
	B	110.1	114.9	115.4	112.0	119.8	120.5
C_{anth} inv. [Gt C]	N	736	736	734	736	734	731
	B	815	814	814	814	813	813
total diss. [Gt yr^{-1}]	N	0.13	0.13	0.12	0.13	0.12	0.11
	B	0.58	0.52	0.53	0.56	0.48	0.48
(c) 1000 yr							
TALK grad. [µmol L^{-1}]	N	−37.9	−35.9	−46.3	−29.3	−20.5	−13.0
	B	8.5	7.3	5.7	11.2	11.2	7.4
C_{anth} inv. [Gt C]	N	2590	2591	2588	2575	2562	2558
	B	3123	3125	3138	3105	3091	3115
total diss. [Gt yr^{-1}]	N	0.17	0.17	0.17	0.17	0.16	0.16
	B	1.08	1.08	1.09	1.07	1.06	1.08

BGD
10, 11343–11373, 2013

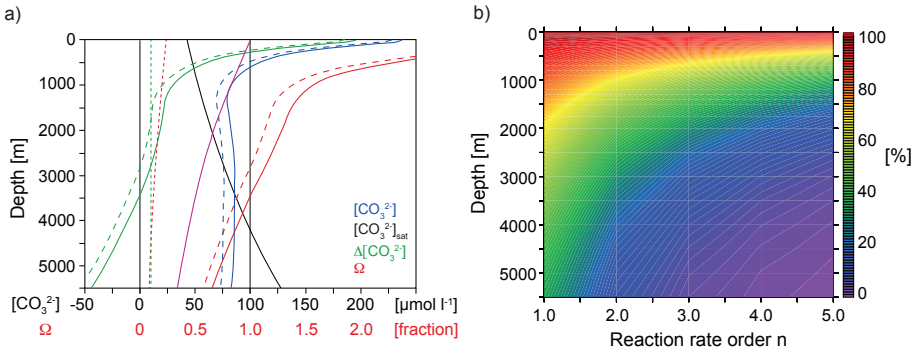

Fig. 1. Sensitivity of the sea water $CaCO_3$ saturation state to ocean acidification. **(a)** Profiles of in-situ $[CO_3^{2-}]$ (blue line) and resulting degree of $CaCO_3$ saturation as given by $\Delta[CO_3^{2-}]$ (green line) and Ω (red line, lower scale). The saturation concentration $[CO_3^{2-}]_{sat}$ is marked by the thick black line. Dashed lines indicate respective changes when reducing the in-situ $[CO_3^{2-}]$ concentration by 10 µmol L^{-1}, mimicking ocean acidification. The dotted lines show the differences between both $\Delta[CO_3^{2-}]$ and Ω before and after "acidification". The decreasing sensitivity of Ω over depth is highlighted by the purple line (lower scale), showing the value of the change in Ω (red dotted line) at each depth relative to the surface. **(b)** Sensitivity of the $CaCO_3$ dissolution reaction rate to ocean acidification, using $S = (1 - \Omega)^n$ in Eq. (5), as a function of the reaction rate order n and depth. The value is calculated by relating the sensitivity of the expression $(1 - \Omega)^n$ to $[CO_3^{2-}]$ (Eq. 6) from each depth to the respective value at the sea surface (Eq. 7). All values calculations are based on the GLODAP data set (Key et al., 2004).

BGD
10, 11343–11373, 2013

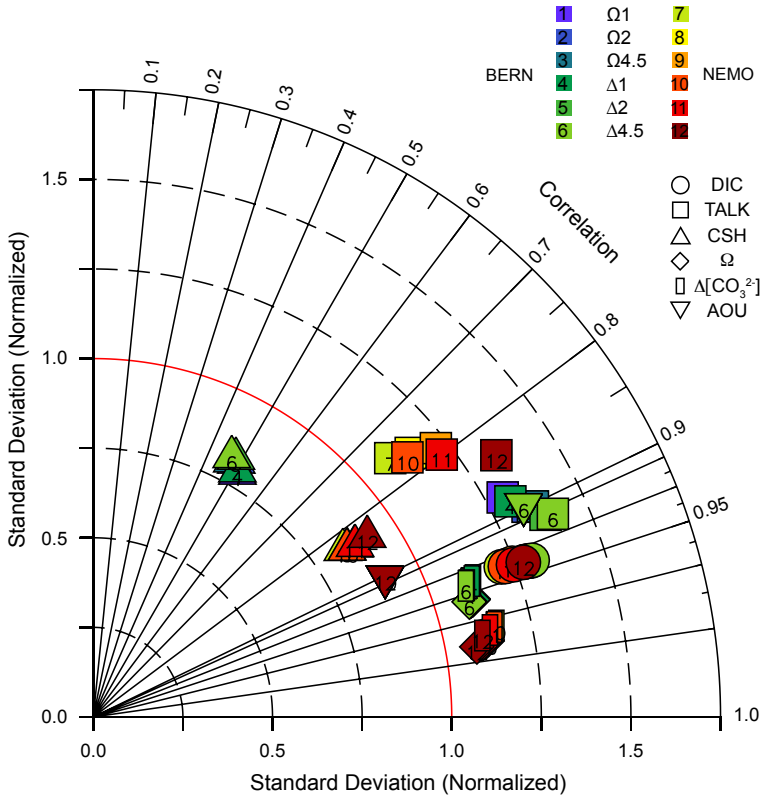

Fig. 2. Taylor diagram illustrating the correspondence between model results and observation based estimates (Key et al., 2004; Takahashi et al., 2009) for total alkalinity (TALK), dissolved inorganic carbon (DIC), saturation state with respect to calcite (Ω, $\Delta[CO_3^{2-}]$), calcite saturation horizon (CSH), and apparent oxygen utilization (AOU).

BGD
10, 11343–11373, 2013

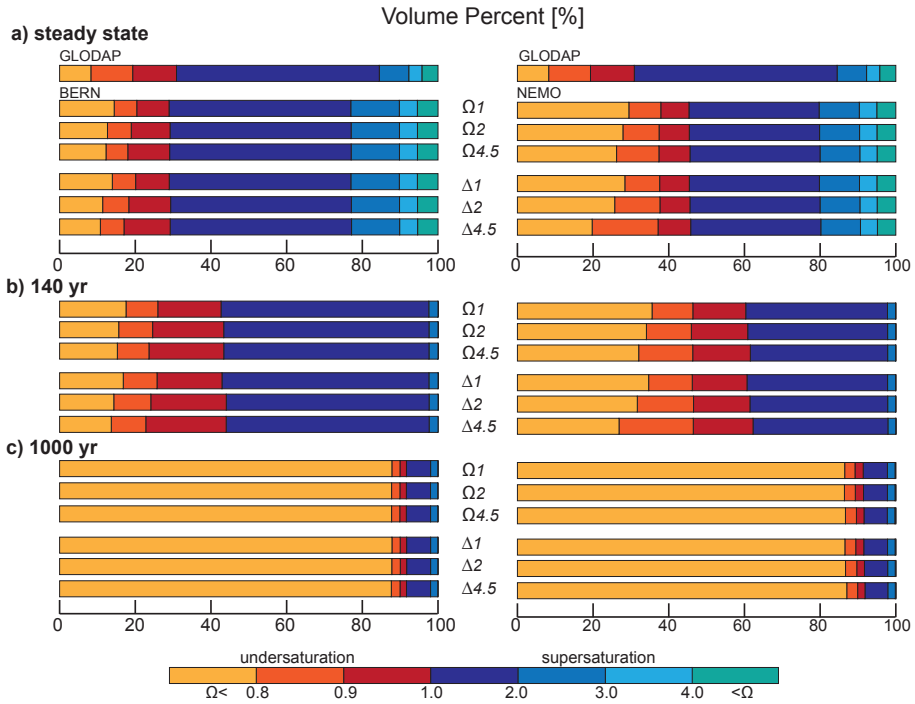

Fig. 3. Distribution of calcite saturation state in the global ocean, as given by the relative volumes (%) of water masses based on Ω. Data is from GLODAP observations (Key et al., 2004) and model results are shown at **(a)** steady state, **(b)** after reaching $4\times CO_2$ (year 140), and **(c)** after 860 yr of stabilization (year 1000).

BGD
10, 11343–11373, 2013

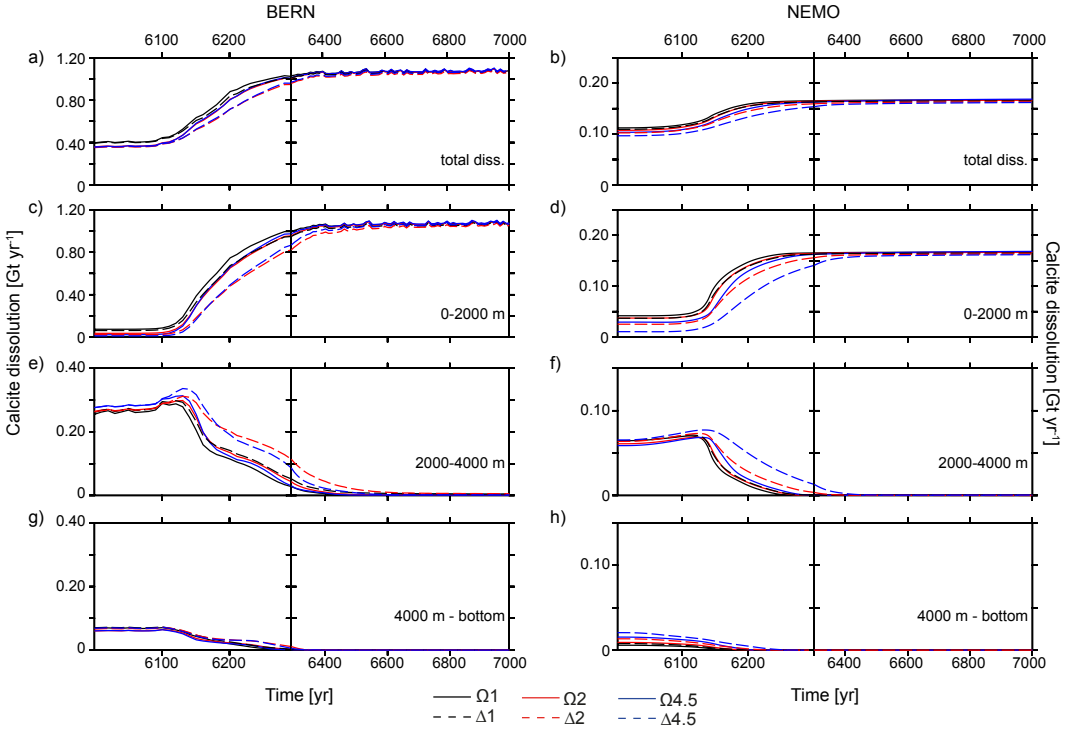

Fig. 4. Integrated calcite dissolution [Gt yr^{-1}] in the BERN model (left) and NEMO model (right). Shown is **(a, b)** total global dissolution; **(c, d)** depth range 0–2000 m; **(e, f)** 2000–4000 m, and **(g, h)** 4000 m–bottom.

BGD
10, 11343–11373, 2013

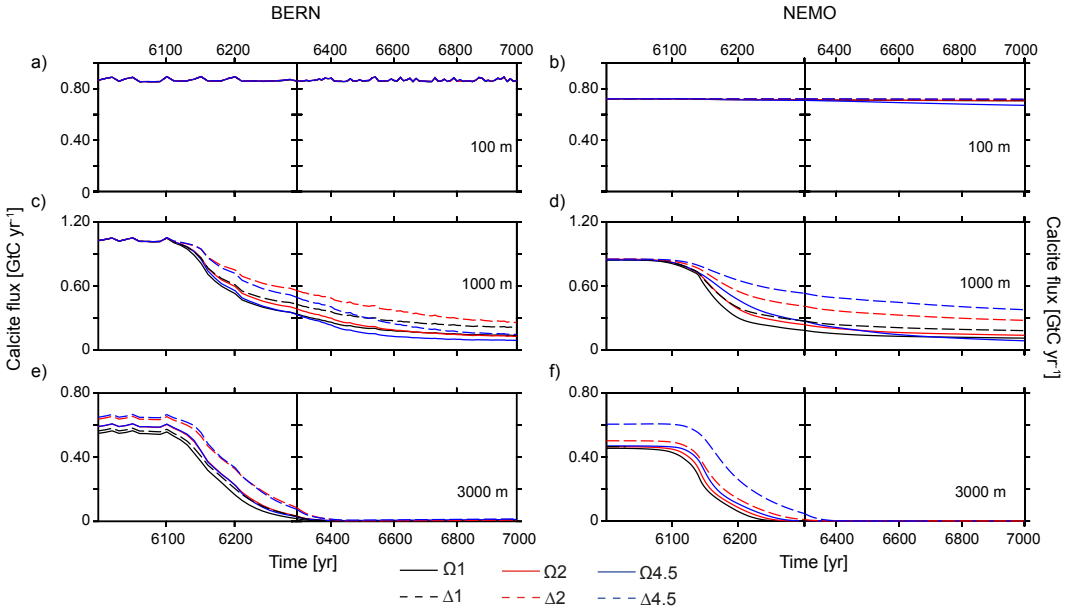

Fig. 5. Globally integrated calcite flux [Gt C yr^{-1}] of all experiments at three different depth levels **(a, b)** 100 m; **(c, d)** 1000 m, and **(e, f)** 3000 m water depth. The BERN model is shown in the left column and the NEMO model in the right column.

BGD
10, 11343–11373, 2013